Environmental Science and Ecotechnology 27 (2025) 100612

Contents lists available at ScienceDirect

Environmental Science and Ecotechnology

journal homepage: www.journals.elsevier.com/environmental-science-and-ecotechnology/

Original Research

Adjoint analysis of $PM_{2.5}$ and O_3 episodes in priority control zones in China

Ruixin Zhang [a,b], Zhihong Chen [c], Xueyan Wu [a,b], Qiming Liu [a,b], Zelin Mai [a,b], Zhiyu Zheng [a,b], Yilin Chen [d], Shu Tao [a,b,e], Yongtao Hu [f], Shunliu Zhao [g], Amir Hakami [g], Armistead G. Russell [f], Huizhong Shen [a,b,*]

[a] State Key Laboratory of Soil Pollution Control and Safety, Shenzhen Key Laboratory of Precision Measurement and Early Warning Technology for Urban Environmental Health Risks, School of Environmental Science and Engineering, Southern University of Science and Technology, Shenzhen, 518055, China
[b] Coastal Atmosphere and Climate of the Greater Bay Area Observation and Research Station of Guangdong Province, Southern University of Science and Technology, Shenzhen, Guangdong, 518055, China
[c] School of Meteorology, University of Oklahoma, Norman, OK, 73019, USA
[d] School of Urban Planning and Design, Peking University Shenzhen Graduate School, Shenzhen, 518055, China
[e] College of Urban and Environmental Sciences, Peking University, Beijing, 100871, China
[f] School of Civil and Environmental Engineering, Georgia Institute of Technology, Atlanta, GA, 30332, USA
[g] Department of Civil and Environmental Engineering, Carleton University, Ottawa, ON, K1S5B6, Canada

ARTICLE INFO

Article history:
Received 8 January 2025
Received in revised form
7 August 2025
Accepted 8 August 2025

Keywords:
Backward sensitivity analysis
Adjoint model
$PM_{2.5}$
Ozone
CMAQ

ABSTRACT

Understanding and mitigating $PM_{2.5}$ and ozone (O_3) pollution remains challenging due to the nonlinear atmospheric chemistry and spatially heterogeneous nature of pollutant emissions. Traditional forward modeling approaches suffer from high computational cost and limited diagnostic resolution to precisely attribute emissions sources at fine spatial, temporal, and chemical scales. Adjoint modeling has emerged as an efficient alternative, enabling high-resolution, multi-pollutant source attribution in a single integrated framework; however, its application to simultaneous $PM_{2.5}$–O_3 pollution episodes is limited, particularly in densely populated regions experiencing complex co-pollutant interactions. Here we apply a newly developed multiphase adjoint of the Community Multiscale Air Quality (CMAQ) model to quantify the emission sensitivities of $PM_{2.5}$ and O_3 concentrations during pollution episodes in major urban agglomerations. Our results indicate that local emissions predominantly drive $PM_{2.5}$ concentrations, contributing up to 79 μg m^{-3}. In contrast, O_3 episodes are largely initiated by regional transport (3.8–7.3 ppbv), surpassing local emission contributions during episode onset. The sensitivity analyses reveal distinct spatial emission signatures and pollutant-specific influences from critical precursors, including volatile organic compounds (VOCs; up to 15.9 ppbv O_3, 11.4 μg m^{-3} $PM_{2.5}$), nitrogen oxides (NO_x; 16.6 ppbv O_3, 13.8 μg m^{-3} $PM_{2.5}$), and ammonia (NH_3; up to 8.7 μg m^{-3} $PM_{2.5}$). This study demonstrates the diagnostic strength and predictive capabilities of adjoint modeling in unraveling complex source–receptor relationships. By offering detailed, pollutant-specific emission sensitivity information, our approach provides a robust foundation for precision-driven emission control strategies and improved cross-regional policy coordination, substantially advancing air quality management frameworks.

© 2025 The Authors. Published by Elsevier B.V. on behalf of Chinese Society for Environmental Sciences, Harbin Institute of Technology, Chinese Research Academy of Environmental Sciences. This is an open access article under the CC BY-NC-ND license (http://creativecommons.org/licenses/by-nc-nd/4.0/).

1. Introduction

Sensitivity analysis methods leverage chemical transport models (CTMs) to elucidate pollution formation mechanisms and support evidence-based policymaking [1–3]. These approaches are broadly categorized into forward and backward frameworks. Traditional forward sensitivity analysis, such as the decoupled

* Corresponding author. State Key Laboratory of Soil Pollution Control and Safety, Shenzhen Key Laboratory of Precision Measurement and Early Warning Technology for Urban Environmental Health Risks, School of Environmental Science and Engineering, Southern University of Science and Technology, Shenzhen, 518055, China.
E-mail address: shenhz@sustech.edu.cn (H. Shen).

https://doi.org/10.1016/j.ese.2025.100612
2666-4984/© 2025 The Authors. Published by Elsevier B.V. on behalf of Chinese Society for Environmental Sciences, Harbin Institute of Technology, Chinese Research Academy of Environmental Sciences. This is an open access article under the CC BY-NC-ND license (http://creativecommons.org/licenses/by-nc-nd/4.0/).

direct method, adopts a source-oriented perspective to assess incremental concentration changes at receptors induced by predefined emission perturbations. However, this method requires multiple simulations or higher-order computations to address nonlinearity, limiting its applicability to prespecified sources [4,5]. Conversely, backward sensitivity analysis, also known as the adjoint method, employs a receptor-oriented paradigm to globally trace sensitivities of predefined cost functions (e.g., concentrations) to all potential sources through a single simulation. Its superior computational efficiency, spatiotemporal attribution capability, and adaptability to complex scenarios (e.g., regional transport, secondary aerosol formation) make it particularly suited for dynamic source tracing in nonlinear systems [6,7].

Owing to its efficiency and flexibility, the adjoint model has become instrumental in analyzing the causation of pollution events and their impacts on population health [8–10]. For instance, Nawaz et al. used the adjoint of the Goddard Earth Observing System with Chemistry (GEOS-Chem) to reveal that emissions from on-road vehicles contributed to 23 % of premature deaths in Washington, D.C., the United States, through particulate matter (PM) with an aerodynamic diameter of 2.5 μm or less ($PM_{2.5}$) [11]. Pappin et al. utilized the adjoint of the Community Multiscale Air Quality Modeling System (CMAQ) to evaluate the health benefits associated with reductions in nitrogen oxide (NO_x) emissions in Canada [12]. Similarly, using the same model, Park et al. found that daytime ozone (O_3) levels in Daegu, South Korea, were more sensitive to transboundary precursors than to local sources [13].

Several studies have applied adjoint models to investigate air pollution dynamics in China. Hu et al. evaluated the Weather Research and Forecasting (WRF) model with chemistry and its adjoint model for optimizing SO_2 emissions in China [14]. The adjoint model achieved a 45.7 % reduction in forecast errors compared with prior emissions, demonstrating its effectiveness in enhancing emission optimization and forecast accuracy. Hu et al. used the GEOS-Chem adjoint to examine $PM_{2.5}$ and O_3 sensitivities in the Yangtze River Delta (YRD) [15]. Wang et al. reported high sensitivity of O_3 in the Beijing–Tianjin–Hebei region to emissions from local and neighboring provinces, including Shandong, Henan, and Jiangsu [16]. Zhai et al. underscored Hebei's significant influence on $PM_{2.5}$ peaks during a severe haze event in Beijing using the Global–Regional Assimilation and Prediction System coupled with the China Meteorological Administration Unified Atmospheric Chemistry Environment adjoint model [17]. In another study using CMAQ-Adjoint, Wang et al. revealed substantial O_3 transport across southern and northern China, and the YRD [18]. While these studies provide valuable insights into regional pollution sources, they typically concentrate on singular locations, specific pollutants, or isolated processes.

Since the launch of the Air Pollution Prevention and Control Action Plan in 2013, China has implemented systematic efforts to reduce air pollution. Key regions such as Jing–Jin–Ji (JJJ), the YRD, and the Pearl River Delta (PRD) were targeted for stricter management due to their dense populations, robust economic activities, and severe pollution levels [19]. Between 2013 and 2017, the $PM_{2.5}$ levels in major cities decreased by 33 %, while sulfur dioxide (SO_2) concentrations decreased by 54 % [20]. The 2018 Three-Year Action Plan to Win the Blue Sky Defense War focused on further reducing emissions, particularly of volatile organic compounds (VOCs) and NO_x [21], which led to further declines in $PM_{2.5}$. However, O_3 pollution has subsequently emerged as a growing challenge [22,23]. In response, the 2023 Opinions on Comprehensively Promoting the Construction of a "Beautiful China" emphasized the need for coordinated control of multiple pollutants and regions [24], signaling a shift toward integrated management [25,26]. Given the frequent co-occurrence of $PM_{2.5}$ and O_3 pollution events and the significant impacts of transboundary transport, mitigating China's complex air pollution landscape requires a tailored approach that is region-specific and temporally adjusted [25,27,28].

In this context, the adjoint model, renowned for its capacity for comprehensive sensitivity analysis, provides critical insights that surpass those achieved through forward model simulations. Despite its potential, the usefulness of adjoint models for comprehensive air pollution assessments involving multiple pollutants and regions remains underexplored. This study employed the latest version of the CMAQ adjoint model, CMAQ-Adjoint v5.0, to assess the dynamic impacts of emissions on $PM_{2.5}$ and O_3 episodes in four priority control regions in China. The objective was to elucidate the contributions of emissions, both within and outside these regions, before and during pollution events, and across various emission species, to inform the development of targeted regional pollution control policies.

2. Materials and methods

2.1. Description of CMAQ-adjoint

The adjoint analysis methodology and the advancements in the CMAQ-Adjoint model are well-documented in previous studies [29,30]. Adjoint analysis entails the computation of gradients of a predetermined cost function (J) relative to all inputs and parameters of the model. Within the context of three-dimensional atmospheric CTMs, J is delineated as follows:

$$J = \int_t \int_x f(c,t,x)\ \mathrm{d}t\ \mathrm{d}x, \tag{1}$$

where c is the concentration field, and x and t are spatial and temporal coordinates, respectively. The adjoint of CTMs is based on the following governing equation:

$$-\frac{\partial \lambda_i}{\partial t} = \nabla\cdot(\mathbf{u}\lambda_i) + \frac{1}{\rho}\nabla\cdot(\rho\mathbf{K}\nabla\lambda_i) + r_i + \frac{\partial f}{\partial c_i}, \tag{2}$$

where λ_i is the adjoint variable of species i ($\lambda_i = \partial J/\partial c_i$); r_i represents the contributions from chemical reaction, thermodynamic transformation, emission, and loss processes for species i; $\partial f/\partial c_i$ denotes the adjoint forcing; $\mathbf{u}$ represents the wind field; ρ is the air density; and $\mathbf{K}$ is the diffusivity tensor [30].

The adjoint model used in this study is a newly developed multiphase adjoint of CMAQ version 5.0 [29]. The model incorporates a discrete adjoint approach for gas-phase chemistry, aerosol formation, cloud chemistry and dynamics, and diffusion processes, while a continuous adjoint technique is utilized for advection. The efficacy and accuracy of the model had undergone extensive evaluations in previous study [29], demonstrating commendable concordance with outcomes derived from forward sensitivity analyses.

2.2. Model configuration

The CMAQ-Adjoint simulation encompasses both forward and backward runs. In the forward phase, the conventional CMAQ model is modified to record the values of active variables pertinent to nonlinear scientific processes, storing these in checkpoint files at each synchronization time step. Subsequently, the backward phase integrates the adjoint equation and reads the checkpoint files to retroactively propagate the adjoint sensitivities backward in time.

The configuration of the WRF-CMAQ-Adjoint model is detailed

in Supplementary Table S1. The latest version of the CMAQ-Adjoint model incorporates the CB05 gas-phase chemical mechanism [31,32] and AERO5 aerosol module [33,34]. The modeling domain encompasses the entire East Asia region (Supplementary Fig. S1), configured with a horizontal grid resolution of 36 km and 13 vertical layers extending up to approximately 16 km above ground level. Similar model configurations have been consistently applied in previous studies [35–37]. The meteorological inputs were generated by the WRF model, version 3.4.1 [38], which leverages global weather forecast data from the National Center for Environmental Prediction. Emission data were sourced from the AiMa emission inventory, which provides comprehensive estimates of anthropogenic emissions, including carbon monoxide (CO), NO_x, VOCs, SO_2, $PM_{2.5}$, PM with aerodynamic diameters of 10 μm or less (PM_{10}), and ammonia (NH_3), across various sectors, such as agriculture, fugitive dust, residential and commercial activities, solvent usage, transportation, biomass burning, industry, and power generation. Emission estimates and associated uncertainties across pollutants are tabulated in Supplementary Table S2, with prior validation studies confirming the inventory's robust performance in simulating atmospheric pollutants over China [35,39,40]. Biogenic emissions were calculated using the Biogenic Emission Inventory System integrated within the CMAQ model [41,42].

2.3. Experimental design

The CMAQ-Adjoint model was employed to elucidate the spatial and temporal dynamics of source contributions to $PM_{2.5}$ and O_3 levels within four densely inhabited regions in China, namely, JJJ, the YRD, the PRD, and the Sichuan Basin (SCB) (Supplementary Fig. S1). This investigation includes an extensive CMAQ forward simulation that encompassed the entirety of 2017, supplemented by 12 targeted short-term CMAQ-Adjoint simulations. The year-long forward simulation serves a dual purpose: It generates pollutant concentration fields for subsequent model validation and establishes initial conditions for the commencement of the short-term adjoint simulations. The evaluation of the model simulation results is provided in Supplementary Text S1, including assessments of meteorological factors (Supplementary Table S3 and Fig. S5–S8), pollutant concentrations (Supplementary Table S4 and Fig. S9–S15), and PM/VOC components (Supplementary Table S5–S6 and Fig. S16–S17).

The short-term CMAQ-Adjoint simulations are specifically designed for each target region, focusing on $PM_{2.5}$ pollution episodes in winter and summer, and O_3 pollution episodes in summer, with the detailed simulation periods listed in Table 1. The key meteorological systems that potentially influence these pollution episodes are characterized in Supplementary Text S2 and Fig. S2–S4. The cost function J for each specified region was delineated as the population-weighted average concentration of $PM_{2.5}$ ($C_{pop,PM_{2.5}}$) or the population-weighted maximum daily 8-h average (MDA8) concentration of O_3 (C_{pop,O_3}) throughout the designated forcing period within the region (equation (3)), using population data from Shen et al. [43]:

$$J = \frac{1}{P}\sum_{i,j} p_{i,j} C_{i,j}, \tag{3}$$

where P denotes the total population within the target region, $p_{i,j}$ represents the population of a specific grid cell, and $C_{i,j}$ corresponds to the average $PM_{2.5}$ or MDA8 O_3 concentration in grid cell (i, j) during the forcing period.

Recognizing that J integrates air pollutants present within the targeted region and during the forcing period, it is crucial to note that the origins of these pollutants may extend beyond regional boundaries or precede the forcing period. Thus, these short-term simulations are characterized by an eight-day active pollution forcing period and a preceding ten-day spin-up phase to ensure a full coverage of the pollution dynamics. The specific durations of the spin-up and forcing periods for each region and pollutant type are detailed in Supplementary Fig. S9–S10. The backward tracking of the adjoint variables revealed the semi-normalized sensitivity of J to emissions from both within and outside the target region, and to emissions occurring before and during the pollution episodes.

The adjoint approach captures the intrinsic local sensitivities [29,30], which vary with emissions if the system is nonlinear. To test the variations in adjoint sensitivities with emission reduction, we conducted additional model experiments with a 30 % reduction in emissions for the winter $PM_{2.5}$ and summer O_3 pollution episodes in the JJJ and the PRD. The results are discussed in subsequent sections and detailed in Supplementary Fig. S18–S23.

3. Sensitivity analysis and key results

3.1. Adjoint analysis of ambient $PM_{2.5}$

3.1.1. Spatial distributions of $PM_{2.5}$ adjoint sensitivity

In the analyzed $PM_{2.5}$ pollution episodes, average concentrations ranged from 33 to 139 μg m^{-3}, with the highest pollution found in the JJJ region and the lowest in the PRD region. $PM_{2.5}$ levels were consistently higher in winter than in summer across all regions.

The local contributions during winter were 78.8, 33.4, 22.0, and 60.9 μg m^{-3} for JJJ, the YRD, the PRD, and the SCB, respectively, compared with 24.3, 14.8, 9.3, and 24.8 μg m^{-3} during summer. Driven by increased industrial activity and heating in northern regions, the local emissions in winter were at least twice those in summer [44,45]. Local emissions dominated $PM_{2.5}$ contributions across the JJJ, the YRD, and the SCB. In JJJ, local sources accounted for 82 % (winter) and 76 % (summer) of $PM_{2.5}$, which aligns with the previously reported 75 % local and 24 % external contributions [46]. Li et al. and Lu et al. suggested lower local contributions for the PRD (20 %–40 %) and the YRD (20 %–70 %) [47,48], which are likely attributable to methodological discrepancies or variability in emission inventories and meteorology. For the SCB, simulations by Qiao et al. align with our analysis, which suggests that 51–83 % of local $PM_{2.5}$ contributions may relate to basin topography

Table 1
Simulation periods of the adjoint for pollution episodes in the target region.

Target region	$PM_{2.5}$		O_3
	Winter	Summer	Summer
JJJ	January 22–January 29	June 27–July 4	June 25–July 2
YRD	February 21–February 28	June 24–July 1	May 25–June 1
PRD	January 21–January 28	July 26–August 2	September 14–September 21
SCB	January 21–January 28	June 28–July 5	July 30–August 6

inhibiting transport and dispersion [49,50].

Regional transport contributions to $PM_{2.5}$ pollution exhibited distinct seasonal patterns. Winter contributions from regional emissions were 17.1, 11.8, 16.6, and 17.2 μg m^{-3} for the JJJ, the YRD, the PRD, and the SCB, respectively, compared with the summer contributions of 7.8, 1.7, 1.0, and 1.3 μg m^{-3}, respectively. Regional transport contributed 24 % to summer $PM_{2.5}$ in JJJ, slightly higher than the 18 % in winter. By contrast, regional transport accounted for larger proportions in winter for the YRD (26 %), PRD (43 %), and SCB (22 %), exceeding the summer contributions of 11 %, 10 %, and 5 %. Similar seasonal patterns of the influence of regional transport have been reported in previous studies. Hou et al., Qu et al., and Li et al. identified lower summer contributions in the YRD, PRD, and SCB [47,51,52]. Chang et al. noted higher contributions from regional transport in the JJJ in July than in January, consistent with our findings, though with higher reported values [53]. The JJJ region was primarily influenced by emissions from Shandong and Henan provinces; the YRD, by Shandong; the PRD, by other regions of Guangdong province, Jiangxi, and Fujian; and the SCB, mainly by Hunan and Hubei (see Fig. 1).

3.1.2. Temporal trends of $PM_{2.5}$ adjoint sensitivity

Adjoint sensitivity analysis using the model time step enabled us to obtain the temporal trend of emission contributions to $C_{pop,PM_{2.5}}$. The regional transport and local emissions were further divided into before and within episodes, with Fig. 2 showing the daily trends of the emission contributions to $C_{pop,PM_{2.5}}$ in the two episodes. Emissions occurring before the pollution events contributed 3 %–16 % of $C_{pop,PM_{2.5}}$, while emissions during the events accounted for 84 %–97 %. Most of the contribution from pre-event emissions came from emissions released one to two days before the event. Emissions from more than six days before the events were negligible (<0.1 %; Table 2).

A further breakdown into local and regional sources indicated that for pollution episodes in the JJJ and the YRD, local emissions had a significantly higher impact on $C_{pop,PM_{2.5}}$ than regional transport, both before and during the pollution events. The aggregate impact of local emissions on $C_{pop,PM_{2.5}}$ before the episodes ranged from 0.5 to 5.7 μg m^{-3}, escalating from 7.9 to 74.7 μg m^{-3} during the episodes. The peak daily contribution of local emissions before the episodes ranged from 0.6 to 4.0 μg m^{-3}, increasing to 2.4 μg m^{-3} during the episodes, and reaching up to 15.3 μg m^{-3}. These results indicate the preeminent influence of local emissions on $PM_{2.5}$ pollution events in the JJJ and the YRD.

The summer pollution episode in PRD exhibited contribution patterns akin to those observed in the JJJ and the YRD, where local emissions were identified as the principal contributors. However, during winter pollution episodes in PRD, the contribution of

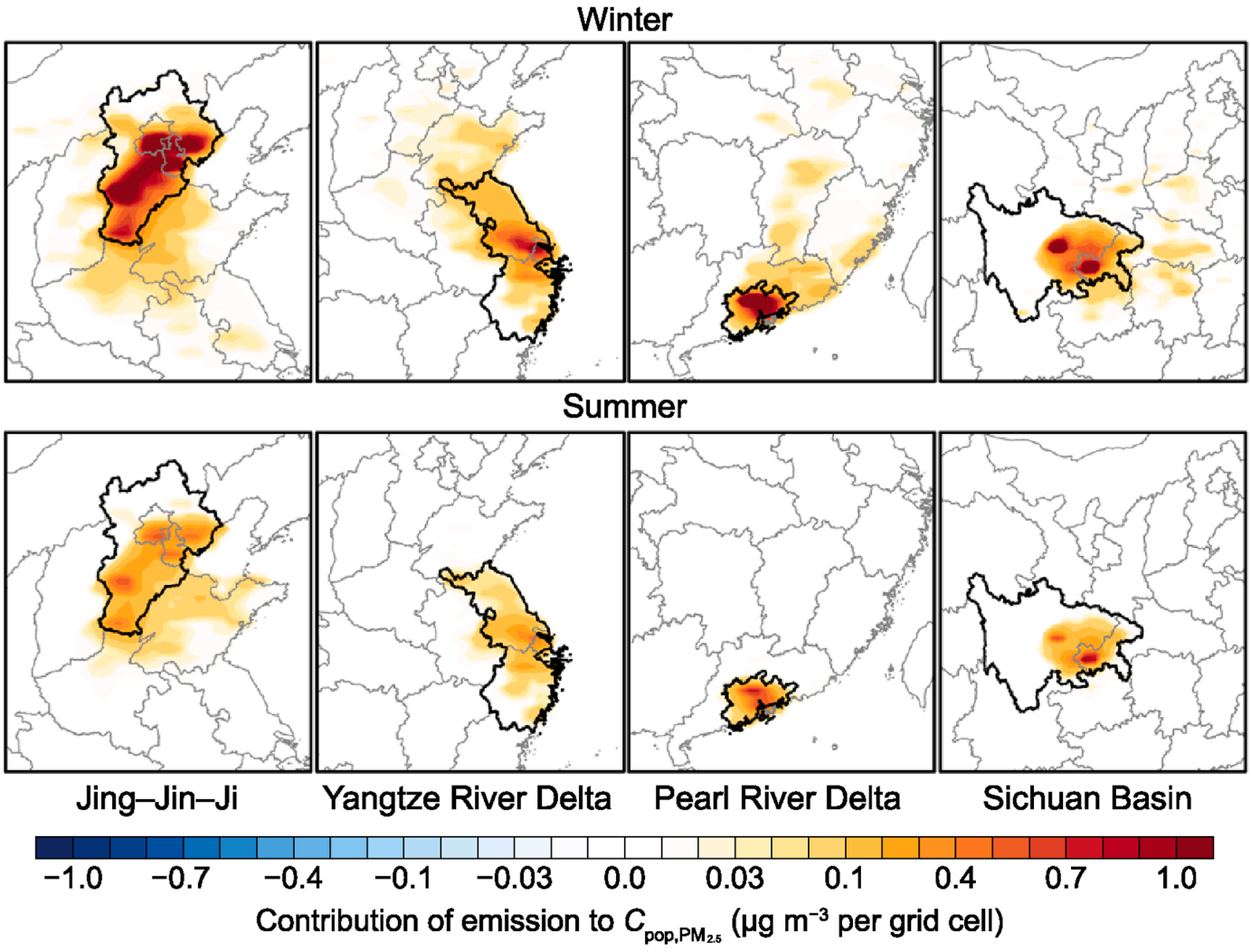

Fig. 1. Spatial distributions of the emission contributions to the population-weighted average concentration of $PM_{2.5}$ ($C_{pop,PM_{2.5}}$) at the four regions in two pollution episodes.

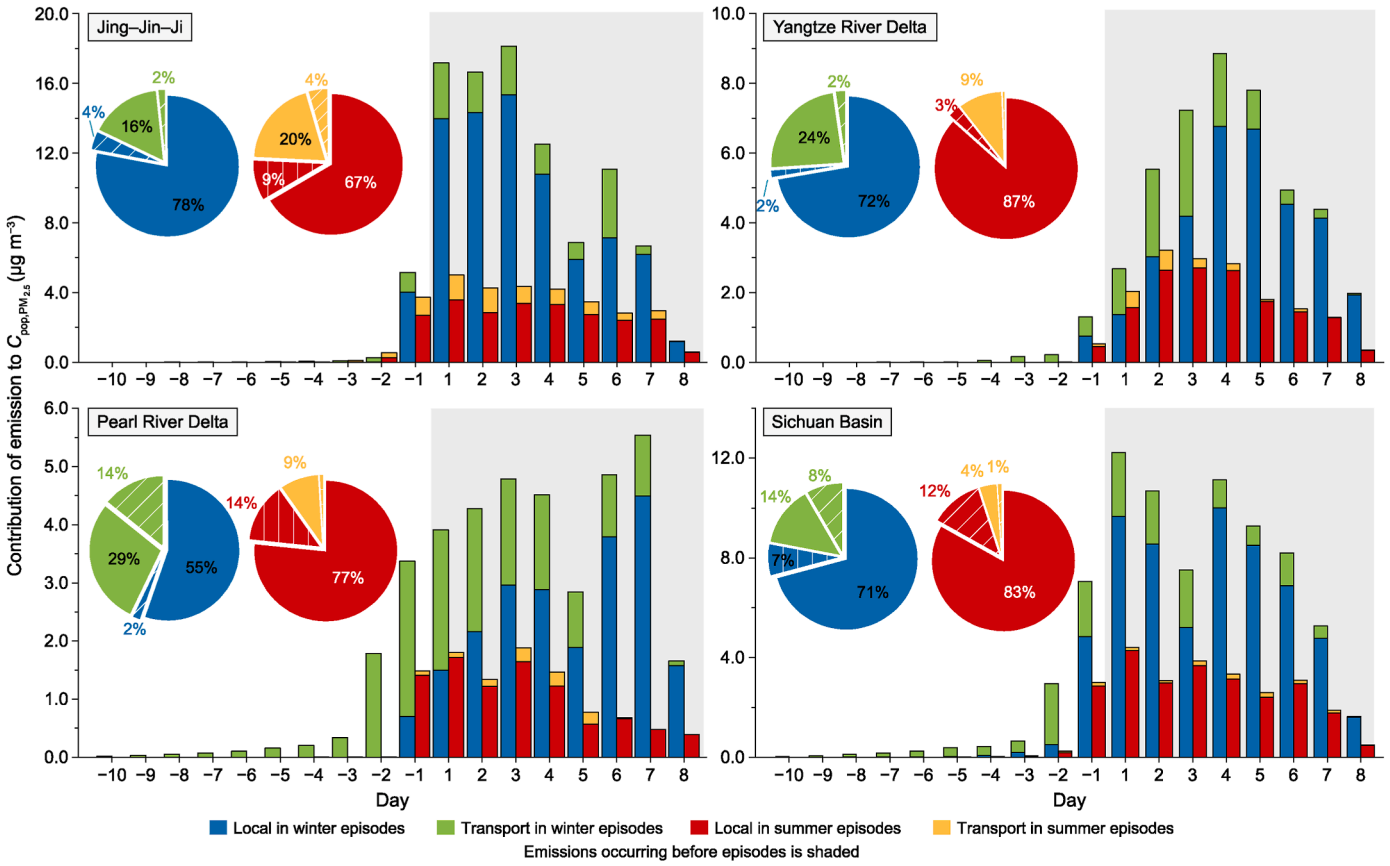

Fig. 2. Temporal trends of the emission contributions to the population-weighted average concentration of $PM_{2.5}$ ($C_{pop,PM_{2.5}}$) at the four regions in two pollution episodes. The negative days represent spin-up days, and the pie chart shows the contribution of different emissions during the entire episode. "Local" represents local emissions, and "transport" represents transboundary transport. Gray shading denotes the active pollution forcing period.

Table 2
Emission contributions to $\boldsymbol{C_{pop,PM_{2.5}}}$ in two forcing periods.

Emissions occurring	JJJ		YRD		PRD		SCB	
	Winter	Summer	Winter	Summer	Winter	Summer	Winter	Summer
Within episode	90.2 (78.0 %)	27.6 (66.5 %)	43.4 (72.2 %)	16.0 (86.7 %)	32.4 (55.2 %)	8.8 (76.6 %)	66.0 (70.7 %)	22.8 (83.2 %)
Before episode	5.6 (4.2 %)	4.4 (9.3 %)	1.8 (1.7 %)	0.6 (2.8 %)	6.1 (1.8 %)	1.5 (13.6 %)	12.1 (7.3 %)	3.3 (11.9 %)
Within one to two days ahead	5.4 (4.2 %)	4.3 (9.2 %)	1.5 (1.7 %)	0.5 (2.8 %)	5.2 (1.8 %)	1.5 (13.6 %)	10.0 (6.9 %)	3.2 (11.7 %)
Six or more days ahead	0.0 (0.0 %)	0.0 (0.0 %)	0.0 (0.0 %)	0.0 (0.0 %)	0.3 (0.0 %)	0.0 (0.0 %)	0.6 (0.0 %)	0.0 (0.0 %)

Note: Unit: μg m^{-3}. The contribution rates of local emissions in the corresponding period are shown in brackets.

regional transport increased compared with those during summer, accounting for 14 % before the episode and 29 % during the episode, closely following the local emission contribution of 55 % within the episode. The maximum daily influence of local emissions on $C_{pop,PM_{2.5}}$ was at 0.7 μg m^{-3} before the episode, surging to 4.5 μg m^{-3} during the episode. Meanwhile, regional transport contribution was at 2.7 μg m^{-3} before the episode and 2.4 μg m^{-3} during the episode, underscoring the critical role of regional transport in precipitating winter $PM_{2.5}$ pollution events likely driven by meteorological transport. These regional transport contributions maintained a significant impact throughout the pollution episode.

The winter pollution episode presented a different scenario in the SCB, with local and regional emissions contributing 7 % and 8 % before the episode, respectively. During the episode, local emissions accounted for 71 % of the pollution, significantly outpacing regional transport, which contributed 14 %. The peak daily contributions from local and regional sources were 6.8 and 3.0 μg m^{-3}, respectively. These findings highlight that both regional emissions and meteorological transport triggered the winter $PM_{2.5}$ pollution events in the SCB, with the accumulation of pollutants intensifying owing to local emissions.

3.1.3. *Compound profiles of $PM_{2.5}$ adjoint sensitivity*

CMAQ-Adjoint remains an indispensable instrument for delineating compound-specific emission contributions, providing detailed sensitivities of the cost function to the emissions of each species, an analysis not readily achievable with conventional

forward models, such as CMAQ or the CMAQ direct decoupled method. Descriptions and classifications of the model species are provided in Supplementary Table S7.

Primary PM was identified as the principal contributor to $C_{pop,PM_{2.5}}$ across all target regions in both winter and summer episodes (see Fig. 3). Contributions ranged from 27.4 to 79.5 μg m^{-3} in winter and from 8.0 to 20.5 μg m^{-3} in summer, with proportional contributions ranging from 49 % to 73 %. Previous studies have reached comparable conclusions: Li et al. identified primary $PM_{2.5}$ emissions as the dominant source in five core cities of the PRD region in 2017 [54], while Xu et al. reported 60 % contributions from direct PM emissions in the JJJ region during the period 2013–2016 [55]. Yang et al. further quantified an average 53 % contribution of primary $PM_{2.5}$ in the PRD region, with contributions reaching 60 % during pollution episodes [56]. Nevertheless, despite its frequent application, the CMAQ-adjoint framework integrating the CB05 chemical mechanism and AERO5 aerosol scheme exhibited limited secondary organic aerosol (SOA) yields from VOCs [57,58]. This constraint may lead to an underestimation of SOA contributions to $PM_{2.5}$ in sensitivity analyses. The key contributing species within the primary PM include $PM_{2.5}$ (PMFINE), organic carbon (POC), elemental carbon (PEC), and sulfate ion (PSO_4). The contributions of specific model species to $C_{pop,PM_{2.5}}$ are detailed in Supplementary Table S8 and Fig. S24.

In most pollution episodes, NO_x emissions facilitated the formation of secondary $PM_{2.5}$, contributing moderately, with values ranging from 2.0 to 13.8 μg m^{-3}. In JJJ, during winter, local NO_x emissions appeared to inhibit $PM_{2.5}$ generation. This phenomenon could be linked to the increase in local NO_x emissions during the winter, which led to elevated NO_x concentrations, a reduction in atmospheric O_3 oxidation capacity, and a consequent diminishment of secondary $PM_{2.5}$ formation capabilities [59].

VOCs were instrumental in the generation of secondary $PM_{2.5}$ in both JJJ and the YRD (Supplementary Fig. S24), with predominant VOC species, including xylene and other polyalkyl aromatics (XYL), internal olefin carbon bond (IOLE), terminal olefin carbon bond (OLE), and toluene and other monoalkyl aromatics (TOL). The impact of VOCs was notably less in summer than in winter, likely due to the heightened photochemical activity in the warmer season, which integrates more VOCs into the photochemical reaction cycle, thereby reducing SOA production [60]. By contrast, VOCs contributions to SOA formation in the PRD and the SCB were comparatively minor.

The SO_2 contributions to $C_{pop,PM_{2.5}}$ across the four target regions were relatively minor, ranging from 0.6 to 1.8 μg m^{-3}, which underscores the efficacy of SO_2 emission control strategies. Zheng et al. demonstrated that SO_2 exhibited the most pronounced reduction, by approximately 62 %, in anthropogenic emissions among major pollutants from 2010 to 2017, a decline consistent with the diminished role of SO_2 in $PM_{2.5}$ formation as quantified by both model simulations and observations [61–63]. Nevertheless, sustained implementation of stringent SO_2 emission controls remains imperative to ensure long-term $PM_{2.5}$ pollution improvements.

NH_3 enhanced secondary $PM_{2.5}$ formation in four regions. In JJJ, NH_3 contributions were marginally higher during summer events than during winter events, whereas in the other three regions, the winter contributions of NH_3 were more pronounced. In the YRD, after primary PM, NH_3 emerged as the second largest contributor to $PM_{2.5}$, with a contribution of 8.7 μg m^{-3}. The PRD region also

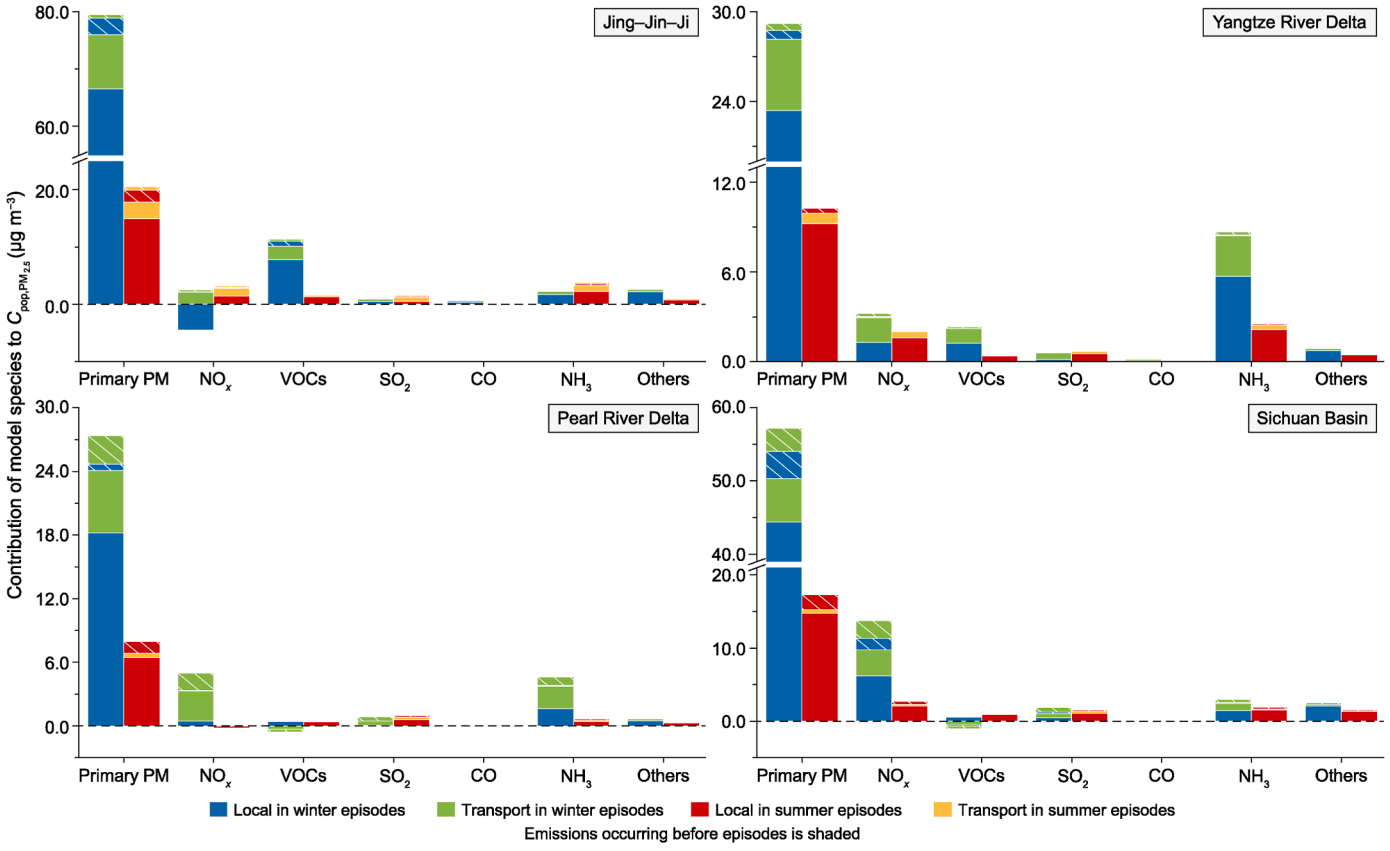

Fig. 3. Contributions of different species to the population-weighted average concentration of $PM_{2.5}$ ($C_{pop,PM_{2.5}}$) at the four regions in two pollution episodes. "Local" represents local emissions, and "transport" represents transboundary transport.

witnessed significant NH_3 contributions during winter events (4.6 μg m^{-3}), with primary PM and NO_x contributions at 27.4 and 5.0 μg m^{-3}, respectively, consistent with results from the study of Han et al. [64]. The results demonstrated that NH_3 emission reduction constitutes a pivotal strategy for further $PM_{2.5}$ mitigation, particularly during winter in the YRD and PRD. This observation aligns with previous studies that confirmed the substantial $PM_{2.5}$ reduction potential of NH_3 emission controls [65,66].

The 30 % emission reduction scenario indicates that the spatial distributions, temporal trends, and compound profiles of emission contributions to $C_{pop,PM_{2.5}}$ remained largely unchanged compared with the reference case (Supplementary Fig. S18–S20). These findings indicate that the response of $PM_{2.5}$ pollution episodes to emission reductions exhibited only moderate nonlinearity.

3.2. Adjoint analysis of ambient O_3

3.2.1. Spatial distributions of O_3 adjoint sensitivity

C_{pop,O_3} in the four target regions was more influenced by regional emissions than $C_{pop,PM_{2.5}}$. The aggregate contributions of emissions to C_{pop,O_3} in JJJ, the YRD, the PRD, and the SCB were 31.1, 16.3, 17.8, and 24.4 μg m^{-3}, respectively, and the proportions of local emissions were 40 %, 34 %, 18 %, and 50 %, respectively. These results indicate that transboundary transport played a more significant role in summer O_3 pollution episodes. Li et al. reported that local emissions contributed 16–42 % to summer ozone in the YRD [67], while Yang et al. found local emission contributions of 43–46 % in PRD [68]. Gao et al. estimated local contributions of 31 %, 32 %, and 41 % in the North China Plain, the YRD, and the PRD, respectively [69]. By contrast, we found a lower local contribution in PRD, approximately 17 %. Shen et al. simulated local emission contributions for 2013–2020, showing 56 %, 69 %, and 67 % in the YRD, PRD, and SCB during summer [70]. Li et al. found that PRD local contributions varied seasonally, from 68 to 80 % in July to 35–55 % in October [71]. These differences highlight the varying impacts of local emissions and regional transport on O_3, influenced by model differences, spatial domains, and study periods, among others [51,72].

Emissions contributing notably to C_{pop,O_3} in the JJJ mainly originated from the Shandong, Henan, and Jiangsu provinces. In the YRD, key contributions were from Anhui and Shandong, while in the PRD, major contributions were from other areas of Guangdong and Jiangxi. In the SCB, emissions from Shaanxi and Henan play an important role. Furthermore, local emissions in the YRD and PRD showed significant negative effects on C_{pop,O_3}, with the maximum negative influence found in the YRD, reaching approximately 0.01 ppbv per grid cell. The adverse impact was even more pronounced in PRD, with a peak reduction exceeding 0.1 ppbv· per grid cell in C_{pop,O_3} (Fig. 4).

3.2.2. Temporal trends of O_3 adjoint sensitivity

Pre-event emissions had a significant impact on C_{pop,O_3} in the target regions, with contributions in the JJJ, the YRD, the PRD, and the SCB amounting to 6.2, 4.3, 6.4, and 8.9 ppbv, respectively (Table 3), accounting for 20 %–37 % of the total emission contribution (Fig. 5). Further breakdown of the pre-event emissions indicated that contributions from the six days before the event ranged from 0.2 to 3.0 ppbv, with a contribution rate of 2 %–12 %. By contrast, emissions from the two days before the event contributed 2.8–3.3 ppbv, with a contribution of 9–20 %.

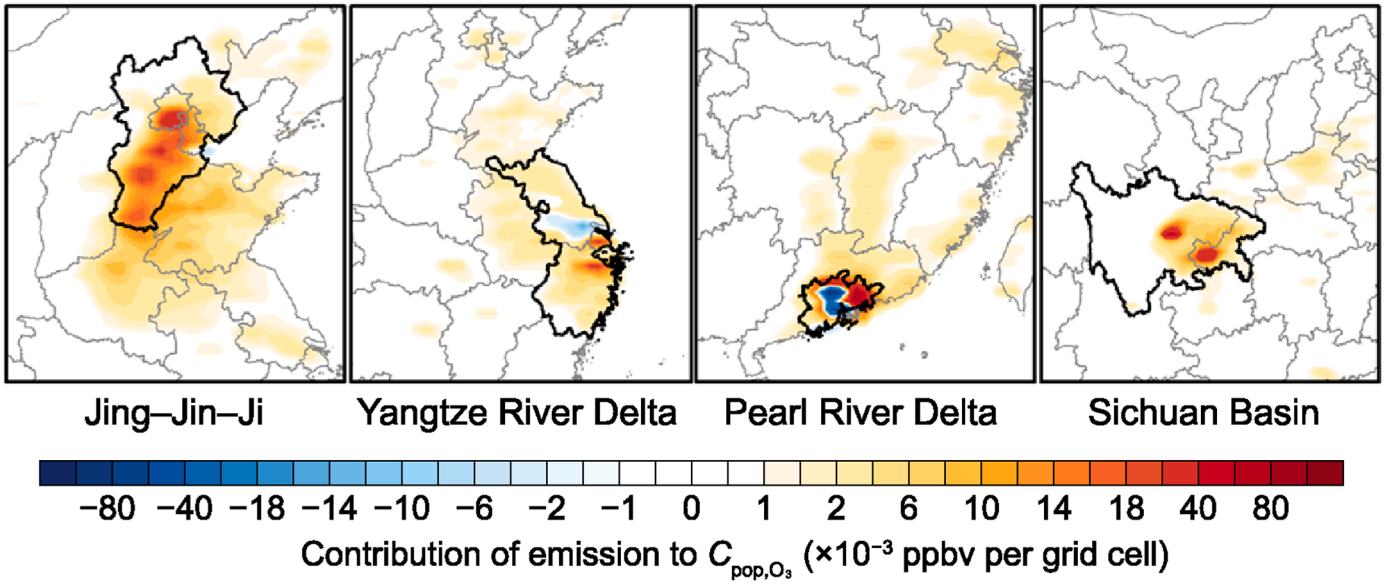

Fig. 4. Spatial distributions of the emission contributions to the population-weighted maximum daily 8-h average (MDA8) concentration of O_3 (C_{pop,O_3}) at the four regions.

Table 3
Emission contributions to C_{pop,O_3} in the forcing periods.

Emissions occurring	JJJ	YRD	PRD	SCB
Within episode	25.0 (36.9 %)	12.0 (30.9 %)	11.4 (16.4 %)	15.5 (43.4 %)
Before episode	6.2 (3.0 %)	4.3 (3.1 %)	6.4 (1.1 %)	8.9 (6.8 %)
Within one to two days ahead	2.9 (2.1 %)	3.3 (2.8 %)	2.8 (0.3 %)	3.2 (4.4 %)
Six or more days ahead	1.1 (0.3 %)	0.2 (0.1 %)	1.7 (0.4 %)	3.0 (0.8 %)

Note: Unit: ppbv. The contribution rates of local emissions in the corresponding period are shown in brackets.

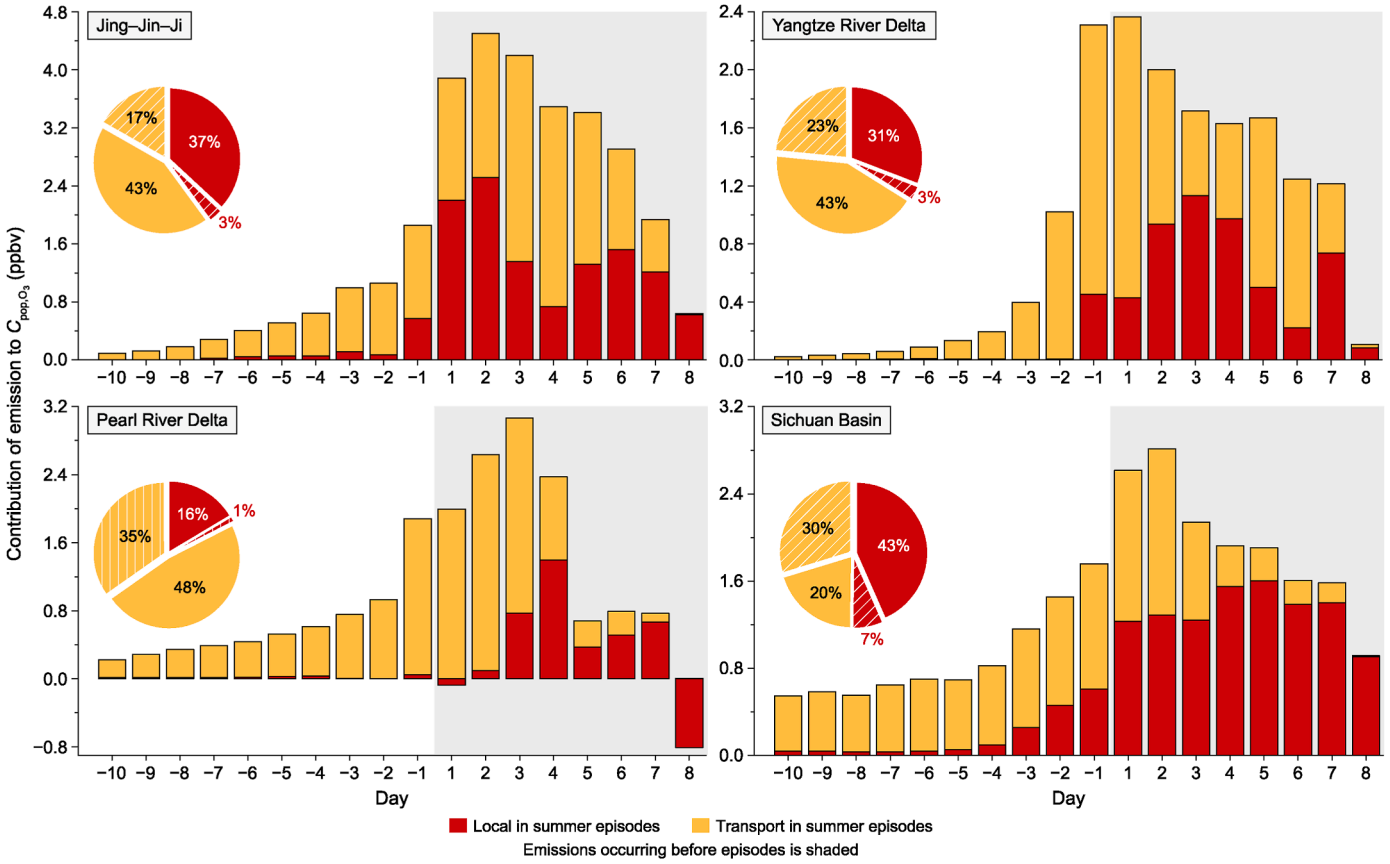

Fig. 5. Temporal trends of the emission contributions to the population-weighted maximum daily 8-h average (MDA8) concentration of O_3 (C_{pop,O_3}) at the four regions. The negative days represent spin-up days, and the pie chart shows the contribution of different emissions during the entire episode. "Local" represents local emissions, and "transport" represents transboundary transport. Gray shading denotes the active pollution forcing period.

To further verify the impacts of pre-event emissions, forward sensitivity tests were conducted in the JJJ and PRD regions, with a 10 % and 30 % reduction in emissions from all sources for the 1–10 days and 6–10 days before the pollution events, respectively. The forward model results aligned with the backward conclusions, confirming the significant role of pre-event emissions (Supplementary Table S9). Moreover, local emissions contributed between 0.2 and 1.7 ppbv, while regional transport contributions accounted for 3.8–7.3 ppbv, highlighting the crucial role of regional transport in triggering O_3 pollution.

Emissions during pollution episodes contributed between 12.0 and 25.0 ppbv to C_{pop,O_3} across the four target regions, representing approximately 63 %–80 % of the total emissions. In the JJJ and the YRD, local emissions contributed 11.5 and 5.0 ppbv, respectively, while regional transport contributed 13.5 and 6.9 ppbv, respectively. These results indicate that regional transport, in combination with local emissions, played a crucial role in sustaining elevated O_3 concentrations throughout the pollution episodes. In PRD, local emissions contributed 2.9 ppbv, while regional transport contributed 8.5 ppbv, nearly three times the contribution from local sources. Regional transport not only initiated the O_3 pollution event but also played a critical role in maintaining high O_3 levels, particularly in the three days leading up to peak pollution. In the SCB, local emissions accounted for 10.6 ppbv, whereas regional transport contributed only 4.9 ppbv. This underscores the dominant role of local emissions in sustaining O_3 pollution in the SCB, in contrast to the more pronounced influence of regional transport in other regions.

3.2.3. *Compound profiles of O_3 adjoint sensitivity*

The primary species that impacted C_{pop,O_3} were NO_x, VOCs, and CO (Fig. 6). In the JJJ and the SCB, regional and local emissions of these species facilitated O_3 formation. VOCs made the most substantial contribution to O_3 levels (15.9 ppbv), followed by NO_x (12.8 ppbv) and CO (2.8 ppbv) in JJJ. In the SCB, NO_x was the leading contributor (16.6 ppbv), with VOCs contributing approximately 7.0 ppbv. The dominant VOC species in both regions were largely consistent, including paraffin carbon bond, OLE, ethene, and internal IOLE. Wang et al., supported by observational data, reached consistent conclusions and further identified olefins as the predominant contributors to O_3 formation in the SCB [73]. In addition, XYL contributed similarly to OLE in JJJ (Supplementary Table S10 and Fig. S25). These species exhibit high photochemical reactivity and significant O_3 production potential.

In the YRD and PRD, VOCs and CO predominantly facilitated O_3 formation, whereas NO_x emissions were associated with a reduction in O_3 levels. VOCs contributions to C_{pop,O_3} in the YRD and PRD amounted to 16.8 and 30.1 ppbv, respectively, with local emissions constituting 73 % and 132 % of these contributions. The spectrum of influential VOC species remained largely consistent across the regions, with the exception that isoprene from biogenic sources had a marginally higher impact in PRD and that XYL was identified as a significant contributor to O_3 formation in both areas [74]. Meanwhile, XYL exhibited significant contributions to summer O_3 formation across all target regions, aligning with findings reported by Shi et al. [75]. The impact of CO on C_{pop,O_3} was considerably less pronounced than that of VOCs, contributing approximately 2.0 and 2.6 ppbv, respectively. NO_x (mainly NO) emissions, particularly

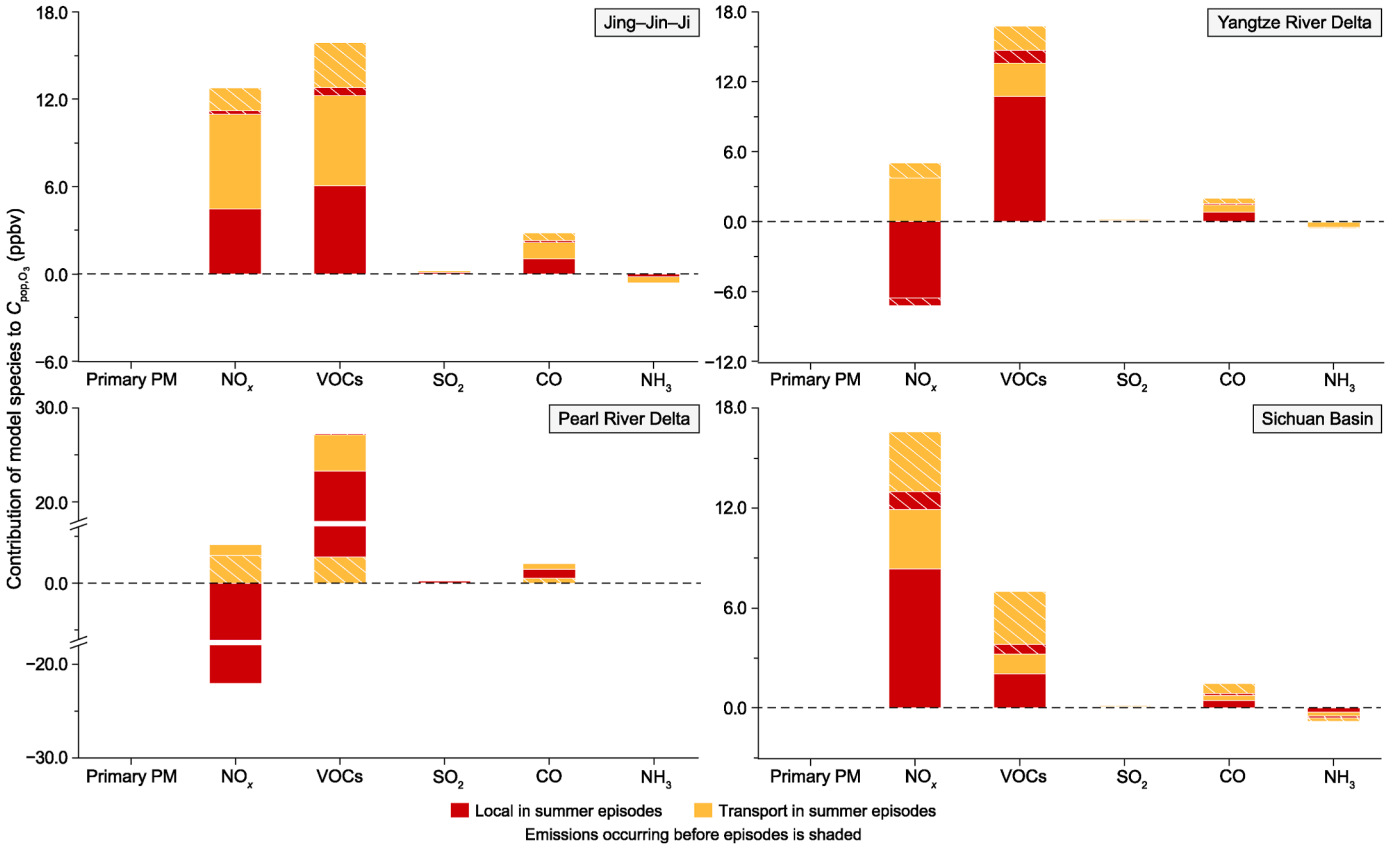

Fig. 6. Contributions of different species to the population-weighted maximum daily 8-h average (MDA8) concentration of O_3 (C_{pop,O_3}) at the four regions. "Local" represents local emissions, and "transport" represents transboundary transport.

from local emissions, led to a decrease in C_{pop,O_3} by approximately −2.2 ppbv in the YRD and −15.0 ppbv in PRD.

Further analysis of ozone formation sensitivity in the target region (Supplementary Fig. S26–S27) revealed that during pollution episodes, C_{pop,O_3} in the YRD and PRD exhibited higher sensitivity to VOCs emission, accompanied by NO_x-saturated conditions, manifesting VOC-limited or transitional regimes. Consequently, VOCs emission enhanced O_3 formation in these areas. These findings aligned with previous studies [76,77]. Mao et al. demonstrated transitional ozone formation regimes across most of the YRD from May to September 2017, with VOC-limited regimes dominating in areas of high anthropogenic emissions [78]. Meanwhile, Lu et al. identified VOC emission-controlled ozone production in the PRD based on a comprehensive review of previous studies [79]. By contrast, the SCB predominantly fell under a NO_x-limited regime during summer, rendering O_3 more responsive to NO_x variations than to VOCs [80]. JJJ tended to be in a transitional regime and demonstrated greater sensitivity to VOCs than to NO_x [81].

The 30 % emission reduction scenario led to notable alterations in both the spatial distribution and temporal trends of emission contributions to C_{pop,O_3} compared with the reference scenario (Supplementary Fig. S21–S23). In the JJJ, the pre-event emissions contributed 11.4 ppbv to C_{pop,O_3}, which decreased to 4.7 ppbv, while the emission contributions during the pollution episode declined from 38.5 to 20.0 ppbv. In PRD, the spatial extent of O_3 depletion from local emissions significantly diminished, with the maximum negative contribution in the grid decreasing from >0.1 ppbv per grid cell to approximately 0.02 ppbv per grid cell. The contribution of pre-event emissions to C_{pop,O_3} in PRD decreased from 12.6 to 4.6 ppbv, and the contribution during the episode decreased from 20.0 to 12.0 ppbv. These results highlight the distinctly nonlinear response of O_3 pollution episodes to emission reductions in certain target regions.

4. Discussion and policy implications

Since 2017, China has pursued a strategic shift toward synergistic $PM_{2.5}$-O_3 control in air quality management. Supported by systematic control policies and stringent pollution mitigation measures, China has achieved notable improvements in ambient air quality, although continued efforts are required for full pollution control. The spatiotemporal and species-resolved backward adjoint modeling framework developed in this study offers novel methodologies and insights for advancing regionally targeted pollution governance.

In the JJJ, local emissions contributed approximately 80 % of $PM_{2.5}$ and 40 % of O_3 pollution, emphasizing the need for targeted local controls. Reducing primary $PM_{2.5}$ emissions requires stricter enforcement of ultra-low emission standards in key industries and production restrictions during pollution episodes, alongside accelerated adoption of clean heating and the phasing out of scattered coal combustion in residential areas. O_3 mitigation requires prioritized abatement of ozone-sensitive VOCs, such as OLE, IOLE, and XYL, through enhanced emission capture and treatment in both industrial process units and solvent-dependent operations. In addition, emissions from Shandong and Henan significantly influenced air quality in the JJJ, underscoring the necessity for enhanced regional cooperation to address both local and transboundary pollution.

In the YRD, $PM_{2.5}$ pollution predominantly originated from local emissions (74 % in winter and 90 % in summer). Exceeded only by primary PM, NH_3 emissions constituted 13 % of $PM_{2.5}$ pollution, demanding urgent implementation of sector-specific controls, such as agricultural strategies that prioritize organic fertilizer adoption and closed-loop livestock management, and rigorous selective catalytic reduction system monitoring coupled with accelerated electrification/hydrogen fuel transitions in the transportation sector. Regional transport contributed 66 % of O_3 pollution, with Shandong and Anhui identified as major sources, reinforcing the importance of early regional coordination in mitigating the adverse impacts of transport pollution.

In PRD, regional transport made a substantial contribution to winter $PM_{2.5}$ pollution (43 %) and played a dominant role in summer O_3 pollution (83 %), with substantial NH_3 transport from northwest Guangdong and Jiangxi. Amplified ozone formation surges with pre-event emission, necessitating cross-sector VOC controls through petrochemical upgrades, low-VOC coatings, and transport regulation synergies.

In the SCB, the topography of the basin amplified the role of local emissions in both $PM_{2.5}$ and O_3 pollution. The local contribution to $PM_{2.5}$ was 60.9 μg m^{-3} (78 %) in winter and 24.8 μg m^{-3} (95 %) in summer. The key pollutants included primary PM and NO_x, with winter contributions exceeding 70 μg m^{-3} and summer contributions surpassing 20 μg m^{-3}. The persistence of O_3 pollution was predominantly driven by local emissions, which contributed approximately 50 % of the pollution episodes. Control strategies should prioritize NO_x and alkene mitigation through industrial low-NO_x combustion, vehicle emission upgrades, petrochemical process optimization, and solvent control while strengthening localized emission reduction.

These findings underscore the necessity for regionally coordinated and spatially tailored pollution control strategies. Implementing customized emission reduction guidelines and strengthening interjurisdictional collaboration are imperative, particularly for addressing O_3 pollution. Enhanced NH_3 emission controls in Eastern China, coupled with targeted abatement of key VOCs, would significantly improve regional air quality while advancing broader pollution mitigation objectives.

The spatiotemporal and species-resolved source contributions presented in this study are emission-dependent during pollution episodes. The 30 % emission abatement scenario demonstrates geographically heterogeneous sensitivity of $PM_{2.5}$ and O_3 to precursor reductions, with O_3 exhibiting pronounced nonlinearity. Moreover, the adjoint model's application of the CB05 gas chemical mechanism and AERO5 aerosol mechanism introduces inherent constraints in representing SOA formation pathways, systematically underestimating SOA contributions to $PM_{2.5}$. Future implementations should incorporate advanced chemical mechanisms to enhance SOA simulation fidelity.

CRediT authorship contribution statement

Ruixin Zhang: Writing – review & editing, Writing – original draft, Visualization, Validation, Investigation, Formal analysis. **Zhihong Chen:** Writing – original draft, Validation, Investigation, Formal analysis. **Xueyan Wu:** Writing – review & editing, Visualization, Validation, Methodology, Data curation. **Qiming Liu:** Writing – review & editing, Validation, Methodology. **Zelin Mai:** Writing – review & editing, Visualization, Validation, Methodology. **Zhiyu Zheng:** Writing – review & editing, Validation, Methodology. **Yilin Chen:** Writing – review & editing, Supervision, Investigation, Data curation. **Shu Tao:** Writing – review & editing, Supervision, Funding acquisition. **Yongtao Hu:** Writing – review & editing, Methodology, Formal analysis, Conceptualization. **Shunliu Zhao:** Writing – review & editing, Software, Conceptualization. **Amir Hakami:** Writing – review & editing, Software, Conceptualization. **Armistead G. Russell:** Writing – review & editing, Supervision, Funding acquisition, Conceptualization. **Huizhong Shen:** Writing – review & editing, Writing – original draft, Visualization, Validation, Supervision, Methodology, Investigation, Funding acquisition, Formal analysis, Conceptualization.

Declaration of competing interest

The authors declare that they have no known competing financial interests or personal relationships that could have appeared to influence the work reported in this paper.

The author is an Editorial Board Member/Editor-in-Chief/Associate Editor/Guest Editor for this journal and was not involved in the editorial review or the decision to publish this article.

Acknowledgments

This research is supported by the National Natural Science Foundation of China (42475108), the Ministry of Science and Technology of the People's Republic of China (2023YFE0112901), Shenzhen Science and Technology Program (KQTD20240729102048052), the National Natural Science Foundation of China (42192512 and 42207116), the Shenzhen Key Laboratory of Precision Measurement and Early Warning Technology for Urban Environmental Health Risks (ZDSYS20220606100604008), Shenzhen Science and Technology Program (JCYJ20241202152804007 and JCYJ20220818100611024), High-level University Special Fund (G03034K006) and Center for Computational Science and Engineering at Southern University of Science and Technology.

Appendix A. Supplementary data

Supplementary data to this article can be found online at https://doi.org/10.1016/j.ese.2025.100612.

References

[1] M.D. Turner, D.K. Henze, A. Hakami, S. Zhao, J. Resler, G.R. Carmichael, C. O. Stanier, J. Baek, A. Sandu, A.G. Russell, et al., Differences between magnitudes and health impacts of BC emissions across the United States using 12 km scale seasonal source apportionment, Environ. Sci. Technol. 49 (7) (2015) 4362–4371, https://doi.org/10.1021/es505968b.

[2] X.H. Du, W. Tang, Z.Z. Zhang, Y. Li, Z.S. Xiao, F. Meng, Sensitivity modeling of ozone and its precursors over the Chengdu metropolitan area, Atmos. Environ. 277 (2022), https://doi.org/10.1016/j.atmosenv.2022.119071.

[3] C.D. Wang, W.J. Duan, S.Y. Cheng, K. Jiang, Emission inventory and air quality impact of non-road construction equipment in different emission stages, Sci. Total Environ. 906 (2024), https://doi.org/10.1016/j.scitotenv.2023.167416.

[4] Y.J. Yang, J.G. Wilkinson, A.G. Russell, Fast, direct sensitivity analysis of multidimensional photochemical models, Environ. Sci. Technol. 31 (10) (1997) 2859–2868, https://doi.org/10.1021/es970117w.

[5] A. Hakami, M.T. Odman, A.G. Russell, High-order, direct sensitivity analysis of multidimensional air quality models, Environ. Sci. Technol. 37 (11) (2003) 2442–2452, https://doi.org/10.1021/es020677h.

[6] R. Giering, Tangent linear and Adjoint Model Compiler, Users manual 1.4 (1999). http://www.autodiff.com/tamc. (Accessed 3 February 2024).

[7] R. Giering, T. Kaminski, Recipes for adjoint code construction, ACM Trans. Math Software 24 (1998) 437–474, https://doi.org/10.1145/293686.293695.

[8] A. Kashfi Yeganeh, M. Momeni, Y. Choi, J. Park, J. Jung, A case study of surface ozone source contributions in the Seoul metropolitan area using the adjoint of CMAQ, J. Air Waste Manag. Assoc. (2024), https://doi.org/10.1080/10962247.2024.2361021.

[9] C.J. Lee, R.V. Martin, D.K. Henze, M. Brauer, A. Cohen, A. Donkelaar, Response of global particulate-matter-related mortality to changes in local precursor emissions, Environ. Sci. Technol. 49 (7) (2015) 4335–4344, https://doi.org/10.1021/acs.est.5b00873.

[10] Y.B. Öztaner, M. Soltanzadeh, S. Zhao, A. Hakami, Health benefits of phasing out coal-fired power plants in Ontario, Alberta, and Canada, Atmos. Environ. 334 (2024), https://doi.org/10.1016/j.atmosenv.2024.120711.

[11] M.O. Nawaz, D.K. Henze, C. Harkins, H. Cao, B. Nault, D. Jo, J. Jimenez, S. C. Anenberg, D.L. Goldberg, Z. Qu, Impacts of sectoral, regional, species, and day-specific emissions on air pollution and public health in Washington, DC, Elementa: Science of the Anthropocene 9 (1) (2021), https://doi.org/10.1525/elementa.2021.00043.
[12] A.J. Pappin, A. Hakami, P. Blagden, M. Nasari, M. Szyszkowicz, R.T. Burnett, Health benefits of reducing NOx emissions in the presence of epidemiological and atmospheric nonlinearities, Environ. Res. Lett. 11 (6) (2016), https://doi.org/10.1088/1748-9326/11/6/064015.
[13] S.-Y. Park, C. Park, J.-W. Yoo, S.-H. Lee, H.W. Lee, Adjoint sensitivity of inland ozone to its precursors and meteorological and chemical influences, Atmos. Environ. 192 (2018) 104–115, https://doi.org/10.1016/j.atmosenv.2018.08.006.
[14] Y. Hu, Y. Li, X. Ma, Y. Liang, W. You, X. Pan, Z. Zang, The optimization of SO2 emissions by the 4DVAR and EnKF methods and its application in WRF-Chem, Sci. Total Environ. 888 (2023), https://doi.org/10.1016/j.scitotenv.2023.163796.
[15] W. Hu, Y. Zhao, N. Lu, X. Wang, B. Zheng, D.K. Henze, L. Zhang, T.M. Fu, S. Zhai, Changing responses of $PM_{2.5}$ and ozone to source emissions in the Yangtze River Delta using the adjoint model, Environ. Sci. Technol. 58 (1) (2024) 628–638, https://doi.org/10.1021/acs.est.3c05049.
[16] X. Wang, T.M. Fu, L. Zhang, H. Cao, Q. Zhang, H. Ma, L. Shen, M.J. Evans, P. D. Ivatt, X. Lu, et al., Sensitivities of ozone air pollution in the beijing-tianjin-hebei area to local and upwind precursor emissions using adjoint modeling, Environ. Sci. Technol. 55 (9) (2021) 5752–5762, https://doi.org/10.1021/acs.est.1c00131.
[17] S. Zhai, X. An, T. Zhao, Z. Sun, W. Wang, Q. Hou, Z. Guo, C. Wang, Detection of critical PM2.5 emission sources and their contributions to a heavy haze episode in Beijing, China, using an adjoint model, Atmos. Chem. Phys. 18 (9) (2018) 6241–6258, https://doi.org/10.5194/acp-18-6241-2018.
[18] M.Y. Wang, S.H.L. Yim, D.C. Wong, K.F. Ho, Source contributions of surface ozone in China using an adjoint sensitivity analysis, Sci. Total Environ. 662 (2019) 385–392, https://doi.org/10.1016/j.scitotenv.2019.01.116.
[19] The State Council of the people's Republic of China. Air pollution prevention and control action plan. https://www.gov.cn/zhengce/content/2013-09/13/content_4561.htm, 2013.
[20] J. Huang, X. Pan, X. Guo, G. Li, Health impact of China's Air Pollution Prevention and Control Action Plan: an analysis of national air quality monitoring and mortality data, Lancet Planet. Health 2 (7) (2018) e313–e323, https://doi.org/10.1016/S2542-5196(18)30141-4.
[21] The State Council of the people's Republic of China. Three-Year action plan to win the blue sky defense War. https://www.gov.cn/zhengce/content/2018-07/03/content_5303158.htm, 2018.
[22] Q. Xiao, G. Geng, T. Xue, S. Liu, C. Cai, K. He, Q. Zhang, Tracking PM2.5 and O3 pollution and the related health burden in China 2013–2020, Environ. Sci. Technol. 56 (11) (2021) 6922–6932, https://doi.org/10.1021/acs.est.1c04548.
[23] X. Zhang, B. Yan, C. Du, C. Cheng, H. Zhao, Quantifying the interactive effects of meteorological, socioeconomic, and pollutant factors on summertime ozone pollution in China during the implementation of two important policies, Atmos. Pollut. Res. 12 (12) (2021), https://doi.org/10.1016/j.apr.2021.101248.
[24] The State Council of the people's Republic of China, Opinions on Comprehensively Promoting the Construction of a “Beautiful China”; Beijing, 2023. https://www.gov.cn/gongbao/2024/issue_11126/202401/content_6928805.html.
[25] K. Li, D.J. Jacob, H. Liao, J. Zhu, V. Shah, L. Shen, K.H. Bates, Q. Zhang, S. Zhai, A two-pollutant strategy for improving ozone and particulate air quality in China, Nat. Geosci. 12 (11) (2019) 906–910, https://doi.org/10.1038/s41561-019-0464-x.
[26] H. Zhao, K. Chen, Z. Liu, Y. Zhang, T. Shao, H. Zhang, Coordinated control of PM2.5 and O_3 is urgently needed in China after implementation of the “Air pollution prevention and control action plan”, Chemosphere 270 (2021) https://doi.org/10.1016/j.chemosphere.2020.129441.
[27] Y. Wang, W. Gao, S. Wang, T. Song, Z. Gong, D. Ji, L. Wang, Z. Liu, G. Tang, Y. Huo, et al., Contrasting trends of $PM_{2.5}$ and surface-ozone concentrations in China from 2013 to 2017, Natl. Sci. Rev. 7 (8) (2020) 1331–1339, https://doi.org/10.1093/nsr/nwaa032.
[28] S. Du, C. He, L. Zhang, Y. Zhao, L. Chu, J. Ni, Policy implications for synergistic management of $PM_{2.5}$ and O_3 pollution from a pattern-process-sustainability perspective in China, Sci. Total Environ. 916 (2024) 170210, https://doi.org/10.1016/j.scitotenv.2024.170210.
[29] S. Zhao, M.G. Russell, A. Hakami, S.L. Capps, M.D. Turner, D.K. Henze, P. B. Percell, J. Resler, H. Shen, A.G. Russell, et al., A multiphase CMAQ version 5.0 adjoint, Geosci. Model Dev. (GMD) 13 (7) (2020) 2925–2944, https://doi.org/10.5194/gmd-13-2925-2020.
[30] A. Hakami, D.K. Henze, J.H. Seinfeld, K. Singh, A. Sandu, S.T. Kim, D.W. Byun, Q.B. Li, The adjoint of CMAQ, Environ. Sci. Technol. 41 (22) (2007) 7807–7817, https://doi.org/10.1021/es070944p.
[31] G. Yarwood, S. Rao, M. Yocke, G.Z. Whitten, Final report - updates to the carbon bond chemical mechanism: CB05, Report Prepared for US EPA RT-04-00675 (2005). Environ: Novato, CA.
[32] D. Luecken, G. Sarwar, G. Yarwood, G.Z. Whitten, W.P.L. Carter, Impact of an updated carbon bond mechanism on predictions from the CMAQ modeling System: preliminary assessment, J. Appl. Meteorol. Climatol. 47 (1) (2008) 3–14, https://doi.org/10.1175/2007jamc1393.1.
[33] A.G. Carlton, P.V. Bhave, S.L. Napelenok, E.D. Edney, G. Sarwar, R.W. Pinder, G. A. Pouliot, M. Houyoux, Model representation of secondary organic aerosol in CMAQv4.7, Environ. Sci. Technol. 44 (22) (2010) 8553–8560, https://doi.org/10.1021/es100636q.
[34] K.M. Foley, S.J. Roselle, K.W. Appel, P.V. Bhave, J.E. Pleim, T.L. Otte, R. Mathur, G. Sarwar, J.O. Young, R.C. Gilliam, et al., Incremental testing of the Community Multiscale Air Quality (CMAQ) modeling system version 4.7, Geosci. Model Dev. (GMD) 3 (1) (2010) 205–226, https://doi.org/10.5194/gmd-3-205-2010.
[35] H. Shen, G. Shen, Y. Chen, A.G. Russell, Y. Hu, X. Duan, W. Meng, Y. Xu, X. Yun, B. Lyu, et al., Increased air pollution exposure among the Chinese population during the national quarantine in 2020, Nat. Hum. Behav. 5 (2) (2021) 239–246, https://doi.org/10.1038/s41562-020-01018-z.
[36] L. Zheng, W. Adalibieke, F. Zhou, P. He, Y. Chen, P. Guo, J. He, Y. Zhang, P. Xu, C. Wang, et al., Health burden from food systems is highly unequal across income groups, Nat. Food 5 (3) (2024) 251–261, https://doi.org/10.1038/s43016-024-00946-7.
[37] Y.L. Chen, H.Z. Shen, G.F. Shen, J.M. Ma, Y.F. Cheng, A.G. Russell, S.L. Zhao, A. Hakami, S. Tao, Substantial differences in source contributions to carbon emissions and health damage necessitate balanced synergistic control plans in China, Nat. Commun. 15 (1) (2024), https://doi.org/10.1038/s41467-024-50327-8.
[38] W.C. Skamarock, J.B. Klemp, J. Dudhia, D.O. Gill, D. Barker, M.G. Duda, J. G. Powers, A Description of the Advanced Research WRF Version 3 (No. NCAR/TN-475+STR), University Corporation for Atmospheric Research, 2008, https://doi.org/10.5065/D68S4MVH.
[39] B. Lyu, Y. Hu, W. Zhang, Y. Du, B. Luo, X. Sun, Z. Sun, Z. Deng, X. Wang, J. Liu, et al., Fusion method combining ground-level observations with chemical transport model predictions using an ensemble deep learning framework: application in China to estimate spatiotemporally-resolved $PM_{2.5}$ exposure fields in 2014-2017, Environ. Sci. Technol. 53 (13) (2019) 7306–7315, https://doi.org/10.1021/acs.est.9b01117.
[40] B. Lyu, Y. Zhang, Y. Hu, Improving PM2.5 air quality model forecasts in China using a bias-correction framework, Atmosphere 8 (8) (2017), https://doi.org/10.3390/atmos8080147.
[41] J.M. Vukovich, T.E. Pierce, The Implementation of BEIS3 within the SMOKE modeling framework. https://www.semanticscholar.org/paper/The-Implementation-of-BEIS3-within-the-SMOKE-Vukovich-Pierce/22e94e5e55a3e86b67e60f3a4b52c6b2c5d8d481#cited-papers, 2002.
[42] S. Arunachalam, Z. Adelman, R. Mathur, J.M. Vukovich, The impacts of biogenic emissions estimates from BEIS-3 on ozone modeling in the Southeastern US. https://www.semanticscholar.org/paper/The-Impacts-of-Biogenic-Emissions-Estimates-from-on-Arunachalam-Adelman/0355b094cbd64481c2a423ca27be8a58c5a8443a, 2002.
[43] H.Z. Shen, S. Tao, Y.L. Chen, P. Ciais, B. Güneralp, M.Y. Ru, Q.R. Zhong, X. Yun, X. Zhu, T.B. Huang, et al., Urbanization-induced population migration has reduced ambient $PM_{2.5}$ concentrations in China, Sci. Adv. 3 (7) (2017), https://doi.org/10.1126/sciadv.1700300.
[44] J. Wang, S. Wang, X. Xu, X. Li, P. He, Y. Qiao, Y. Chen, The diminishing effects of winter heating on air quality in northern China, J. Environ. Manag. 325 (2023), https://doi.org/10.1016/j.jenvman.2022.116536.
[45] Y. Tong, J. Gao, K. Wang, H. Jing, C. Wang, X. Zhang, J. Liu, T. Yue, X. Wang, Y. Xing, Highly-resolved spatial-temporal variations of air pollutants from Chinese industrial boilers, Environ. Pollut. 289 (2021), https://doi.org/10.1016/j.envpol.2021.117931.
[46] Z. Dong, S. Wang, J. Xing, X. Chang, D. Ding, H. Zheng, Regional transport in beijing-tianjin-hebei region and its changes during 2014–2017: the impacts of meteorology and emission reduction, Sci. Total Environ. 737 (2020), https://doi.org/10.1016/j.scitotenv.2020.139792.
[47] R. Li, X. Mei, L. Wei, X. Han, M. Zhang, Y. Jing, Study on the contribution of transport to PM2.5 in typical regions of China using the regional air quality model RAMS-CMAQ, Atmos. Environ. 214 (2019), https://doi.org/10.1016/j.atmosenv.2019.116856.
[48] X. Lu, Y. Chen, Y. Huang, C. Lin, Z. Li, J.C.H. Fung, A.K.H. Lau, Differences in concentration and source apportionment of $PM_{2.5}$ between 2006 and 2015 over the PRD region in southern China, Sci. Total Environ. 673 (2019) 708–718, https://doi.org/10.1016/j.scitotenv.2019.03.452.
[49] X. Qiao, H. Guo, Y. Tang, P. Wang, W. Deng, X. Zhao, J. Hu, Q. Ying, H. Zhang, Local and regional contributions to fine particulate matter in the 18 cities of Sichuan Basin, southwestern China, Atmos. Chem. Phys. 19 (9) (2019) 5791–5803, https://doi.org/10.5194/acp-19-5791-2019.
[50] Z. Shu, T. Zhao, Y. Liu, L. Zhang, X. Ma, X. Kuang, Y. Li, Z. Huo, Q. Ding, X. Sun, et al., Impact of deep basin terrain on PM2.5 distribution and its seasonality over the Sichuan Basin, Southwest China, Environ. Pollut. 300 (2022), https://doi.org/10.1016/j.envpol.2022.118944.
[51] K. Qu, Y. Yan, X. Wang, X. Jin, M. Vrekoussis, M. Kanakidou, G.P. Brasseur, T. Lin, T. Xiao, X. Cai, et al., The effect of cross-regional transport on ozone and particulate matter pollution in China: a review of methodology and current knowledge, Sci. Total Environ. 947 (2024), https://doi.org/10.1016/j.scitotenv.2024.174196.
[52] X. Hou, C.K. Chan, G.H. Dong, S.H.L. Yim, Impacts of transboundary air pollution and local emissions on PM2.5 pollution in the Pearl River Delta region of China and the public health, and the policy implications, Environ. Res. Lett. 14 (3) (2019), https://doi.org/10.1088/1748-9326/aaf493.
[53] X. Chang, S. Wang, B. Zhao, J. Xing, X. Liu, L. Wei, Y. Song, W. Wu, S. Cai, H. Zheng, et al., Contributions of inter-city and regional transport to PM2.5

concentrations in the beijing-tianjin-hebei region and its implications on regional joint air pollution control, Sci. Total Environ. 660 (2019) 1191–1200, https://doi.org/10.1016/j.scitotenv.2018.12.474.
[54] L. Li, J.Y. An, M. Zhou, R.S. Yan, C. Huang, Q. Lu, L. Lin, Y.J. Wang, S.K. Tao, L. P. Qiao, et al., Source apportionment of fine particles and its chemical components over the Yangtze River Delta, China during a heavy haze pollution episode, Atmos. Environ. 123 (2015) 415–429, https://doi.org/10.1016/j.atmosenv.2015.06.051.
[55] H. Xu, Z. Xiao, K. Chen, M. Tang, N. Zheng, P. Li, N. Yang, W. Yang, X. Deng, Spatial and temporal distribution, chemical characteristics, and sources of ambient particulate matter in the beijing-tianjin-hebei region, Sci. Total Environ. 658 (2019) 280–293, https://doi.org/10.1016/j.scitotenv.2018.12.164.
[56] K. Yang, D.-H. Chen, X. Ding, J. Li, Y.-Q. Zhang, T. Zhang, Q.-Y. Wang, J.-Q. Wang, Q. Cheng, H. Jiang, et al., Different roles of primary and secondary sources in reducing PM2.5: insights from molecular markers in Pearl River Delta, South China, Atmos. Environ. 294 (2023), https://doi.org/10.1016/j.atmosenv.2022.119487.
[57] H.O. Pye, D.J. Luecken, L. Xu, C.M. Boyd, N.L. Ng, K.R. Baker, B.R. Ayres, J. O. Bash, K. Baumann, W.P. Carter, et al., Modeling the Current and future roles of particulate organic nitrates in the Southeastern United States, Environ. Sci. Technol. 49 (24) (2015) 14195–14203, https://doi.org/10.1021/acs.est.5b03738.
[58] M.C. Woody, K.R. Baker, P.L. Hayes, J.L. Jimenez, B. Koo, H.O.T. Pye, Understanding sources of organic aerosol during CalNex-2010 using the CMAQ-VBS, Atmos. Chem. Phys. 15 (2015) 26745–26793, https://doi.org/10.5194/acpd-15-26745-2015.
[59] R.-J. Huang, Y. Zhang, C. Bozzetti, K.-F. Ho, J.-J. Cao, Y. Han, K.R. Daellenbach, J. G. Slowik, S.M. Platt, F. Canonaco, et al., High secondary aerosol contribution to particulate pollution during haze events in China, Nature 514 (7521) (2014) 218–222, https://doi.org/10.1038/nature13774.
[60] Y. Wang, Y. Cui, Q. He, J. Fan, Y. Li, K. Liu, L. Guo, X. Wang, Significant impact of VOCs emission from coking and coal/biomass combustion on O_3 and SOA formation in taiyuan, China, Atmos. Pollut. Res. 14 (2) (2023), https://doi.org/10.1016/j.apr.2023.101671.
[61] B. Zheng, D. Tong, M. Li, F. Liu, C. Hong, G. Geng, H. Li, X. Li, L. Peng, J. Qi, et al., Trends in China's anthropogenic emissions since 2010 as the consequence of clean air actions, Atmos. Chem. Phys. 18 (19) (2018) 14095–14111, https://doi.org/10.5194/acp-18-14095-2018.
[62] G. Geng, Q. Zhang, D. Tong, M. Li, Y. Zheng, S. Wang, K. He, Chemical composition of ambient $PM_{2.5}$ over China and relationship to precursor emissions during 2005–2012, Atmos. Chem. Phys. 17 (14) (2017) 9187–9203, https://doi.org/10.5194/acp-17-9187-2017.
[63] H. Li, J. Cheng, Q. Zhang, B. Zheng, Y. Zhang, G. Zheng, K. He, Rapid transition in winter aerosol composition in Beijing from 2014 to 2017: response to clean air actions, Atmos. Chem. Phys. 19 (17) (2019) 11485–11499, https://doi.org/10.5194/acp-19-11485-2019.
[64] X. Han, L. Zhu, M. Liu, Y. Song, M. Zhang, Numerical analysis of agricultural emissions impacts on $PM_{2.5}$ in China using a high-resolution ammonia emission inventory, Atmos. Chem. Phys. 20 (16) (2020) 9979–9996, https://doi.org/10.5194/acp-20-9979-2020.
[65] S. Zhai, D.J. Jacob, X. Wang, Z. Liu, T. Wen, V. Shah, K. Li, J.M. Moch, K.H. Bates, S. Song, et al., Control of particulate nitrate air pollution in China, Nat. Geosci. 14 (6) (2021) 389–395, https://doi.org/10.1038/s41561-021-00726-z.
[66] Y. Chen, L. Zhang, D.K. Henze, Y. Zhao, X. Lu, W. Winiwarter, Y. Guo, X. Liu, Z. Wen, Y. Pan, et al., Interannual variation of reactive nitrogen emissions and their impacts on PM2.5 air pollution in China during 2005–2015, Environ. Res. Lett. 16 (12) (2021), https://doi.org/10.1088/1748-9326/ac3695.
[67] L. Li, J. An, L. Huang, R. Yan, C. Huang, G. Yarwood, Ozone source apportionment over the Yangtze River Delta region, China: investigation of regional transport, sectoral contributions and seasonal differences, Atmos. Environ. 202 (2019) 269–280, https://doi.org/10.1016/j.atmosenv.2019.01.028.
[68] W. Yang, H. Chen, W. Wang, J. Wu, J. Li, Z. Wang, J. Zheng, D. Chen, Modeling study of ozone source apportionment over the Pearl River Delta in 2015, Environ. Pollut. 253 (2019) 393–402, https://doi.org/10.1016/j.envpol.2019.06.091.
[69] M. Gao, J. Gao, B. Zhu, R. Kumar, X. Lu, S. Song, Y. Zhang, B. Jia, P. Wang, G. Beig, et al., Ozone pollution over China and India: seasonality and sources, Atmos. Chem. Phys. 20 (7) (2020) 4399–4414, https://doi.org/10.5194/acp-20-4399-2020.
[70] L. Shen, J. Liu, T. Zhao, X. Xu, H. Han, H. Wang, Z. Shu, Atmospheric transport drives regional interactions of ozone pollution in China, Sci. Total Environ. 830 (2022), https://doi.org/10.1016/j.scitotenv.2022.154634.
[71] Y. Li, A.K.H. Lau, J.C.H. Fung, H. Ma, Y. Tse, Systematic evaluation of ozone control policies using an Ozone Source Apportionment method, Atmos. Environ. 76 (2013) 136–146, https://doi.org/10.1016/j.atmosenv.2013.02.033.
[72] H. Liu, M. Zhang, X. Han, A review of surface ozone source apportionment in China, Atmospheric and Oceanic Science Letters 13 (5) (2020) 470–484, https://doi.org/10.1080/16742834.2020.1768025.
[73] W. Wang, T. Xiong, W. Zhang, B. Luo, D. Wang, X. Jiang, Z. Rao, Y. Jiang, Y. Liu, H. Cheng, et al., Observation and analysis of VOCs in nine prefecture-level cities of Sichuan Province, China, Environ. Monit. Assess. 192 (8) (2020), https://doi.org/10.1007/s10661-020-08360-9.
[74] Z. Xu, Q. Zou, L. Jin, Y. Shen, J. Shen, B. Xu, F. Qu, F. Zhang, J. Xu, X. Pei, et al., Characteristics and sources of ambient Volatile Organic Compounds (VOCs) at a regional background site, YRD region, China: significant influence of solvent evaporation during hot months, Sci. Total Environ. 857 (2023), https://doi.org/10.1016/j.scitotenv.2022.159674.
[75] Y. Shi, J. Ren, Z. Xi, M. Simayi, S. Xie, Identification of key anthropogenic VOC species and sources controlling summer ozone formation in China, Atmos. Environ. 298 (2023), https://doi.org/10.1016/j.atmosenv.2023.119623.
[76] S. Zhu, J. Ma, S. Wang, S. Sun, P. Wang, H. Zhang, Shifts of Formation regimes and increases of atmospheric oxidation led to ozone increase in North China Plain and Yangtze River Delta from 2016 to 2019, J. Geophys. Res. Atmos. 128 (13) (2023), https://doi.org/10.1029/2022jd038373.
[77] Y. Wang, Y. Zhao, Y. Liu, Y. Jiang, B. Zheng, J. Xing, Y. Liu, S. Wang, C.P. Nielsen, Sustained emission reductions have restrained the ozone pollution over China, Nat. Geosci. 16 (11) (2023) 967–974, https://doi.org/10.1038/s41561-023-01284-2.
[78] Y.-H. Mao, S. Yu, Y. Shang, H. Liao, N. Li, Response of summer ozone to precursor emission controls in the Yangtze River Delta Region, Front. Environ. Sci. 10 (2022), https://doi.org/10.3389/fenvs.2022.864897.
[79] H. Lu, X. Lyu, H. Cheng, Z. Ling, H. Guo, Overview on the spatial–temporal characteristics of the ozone formation regime in China, Environ. Sci. J. Integr. Environ. Res.: Process. Impacts 21 (6) (2019) 916–929, https://doi.org/10.1039/c9em00098d.
[80] Y. Chen, M. Wang, Y. Yao, C. Zeng, W. Zhang, H. Yan, P. Gao, L. Fan, D. Ye, Research on the ozone formation sensitivity indicator of four urban agglomerations of China using Ozone Monitoring Instrument (OMI) satellite data and ground-based measurements, Sci. Total Environ. 869 (2023), https://doi.org/10.1016/j.scitotenv.2023.161679.
[81] H. Song, W. Zhao, X. Yang, W. Hou, L. Chen, P. Ma, Ozone sensitivity analysis and ozone Formation regimes division in the beijing–tianjin–hebei Region based on satellite remote sensing data, Atmosphere 14 (11) (2023), https://doi.org/10.3390/atmos14111637.